Incorporating Isolated Molybdenum (Mo) Atoms into Bilayer Epitaxial Graphene on 4H-SiC(0001)

Wen Wan,[†] Hui Li,[‡] Han Huang,[†,*] Swee Liang Wong,[§] Lu Lv,[†] Yongli Gao,[†] and Andrew Thye Shen Wee[§,⊥,*]

[†]Institute of Super-microstructure and Ultrafast Process in Advanced Materials, School of Physics and Electronics, The Central South University, Changsha, Hunan 410083, PR China, [‡]Institute of Physics, Chinese Academy of Sciences, Beijing 100190, PR China, [§]Department of Physics, National University of Singapore, 2 Science Drive 3, 117542 Singapore, and [⊥]Graphene Research Centre, National University of Singapore, Block S14, Level 6 6 Science Drive 2, 117546 Singapore

ABSTRACT

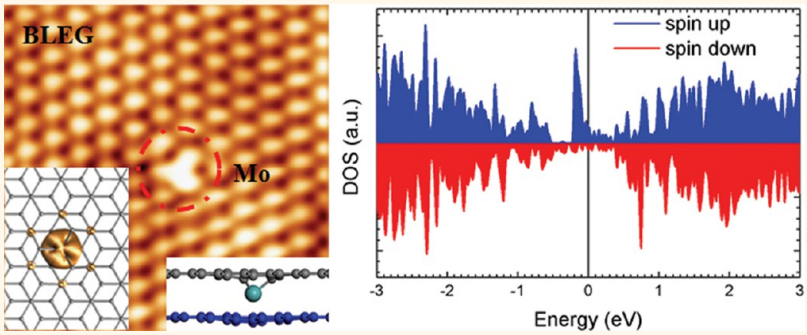

The atomic structures and electronic properties of isolated Mo atoms in bilayer epitaxial graphene (BLEG) on 4H-SiC(0001) are investigated by low temperature scanning tunneling microscopy (LT-STM). LT-STM results reveal that isolated Mo dopants prefer to substitute C atoms at α-sites and preferentially locate between the graphene bilayers. First-principles calculations confirm that the embedding of single Mo dopants within BLEG is energetically favorable as compared to monolayer graphene. The calculated band structures show that Mo-incorporated BLEG is n-doped, and each Mo atom introduces a local magnetic moment of 1.81 μ_B into BLEG. Our findings demonstrate a simple and stable method to incorporate single transition metal dopants into the graphene lattice to tune its electronic and magnetic properties for possible use in graphene spin devices.

KEYWORDS: molybdenum · epitaxial graphene · silicon carbide · scanning tunneling microscopy · density functional theory

Graphene, a one-atom-thick sheet of carbon atoms in honeycomb arrangement, has sparked much interest in both fundamental studies and technological applications in the past 10 years due to its outstanding physical, electronic, and optical properties.[1,2] The development of nanoscale graphene-based devices requires simple methods to tune its electronic and magnetic properties. Impurities and defects, which are always present in crystals, have a strong influence on their electronic, optical, thermal, and mechanical properties. For instance, the conductance of semiconductors and the mechanical strength as well as ductility of metals are governed by defects.[3] Structural defects or dopants (atomic point defects) in graphene have been shown to play an important role in tuning its transport properties.[3,4] Lahiri *et al.* reported the realization of an extended one-dimensional defect embedded in a perfect graphene sheet, which has the potential to act as a conducting wire.[5] Ugeda investigated isolated carbon vacancies in the outermost layer of HOPG and in monolayer graphene on Pt(111) by low temperature scanning tunneling microscopy (LT-STM) (T = 4.2 K).[6,7] They revealed that the vacancies at α sites on HOPG exhibit a much sharper resonance at the Fermi level (E_F) than those at β sites (α sites and β sites are defined in Figure 1), whereas single carbon vacancies in monolayer graphene on Pt(111) exhibit a broad electronic resonance above E_F. This suggests that the magnetic moment associated with carbon vacancies in freestanding

* Address correspondence to physhh@csu.edu.cn, phyweets@nus.edu.sg.

Received for review November 7, 2013 and accepted December 19, 2013.

Published online December 19, 2013
10.1021/nn4057929

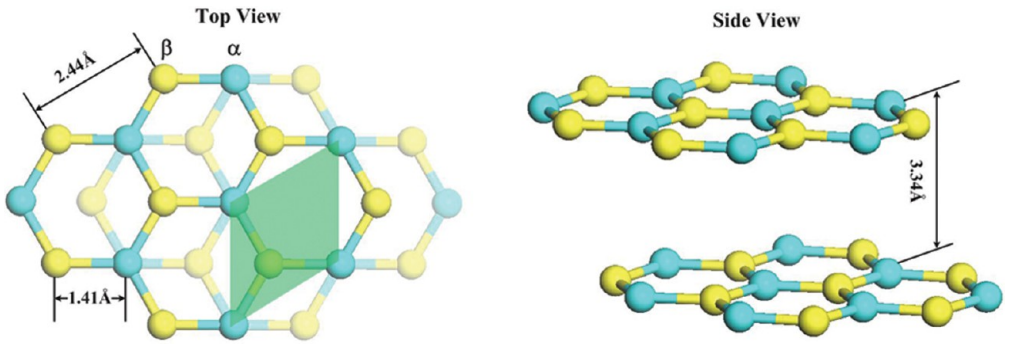

Figure 1. Ball-and-stick model of bilayer graphene showing the two inequivalent carbon atoms (α and β sites) per unit cell. The green diamond highlights the unit cell.

graphene layers can be quenched when graphene hybridizes with the metal substrate at vacancy points. Zhao *et al.* investigated individual nitrogen dopants in monolayer CVD graphene grown on a copper substrate, revealing that individual nitrogen atoms were incorporated as graphitic dopants into graphene and strongly modified its electronic structure, but only within a few lattice spacings from the nitrogen dopant.[8] For comparison, they also reported the local atomic and electronic structures of random boron chemical doping in monolayer CVD graphene in the graphitic form, revealing a contribution of ~0.5 holes into graphene per dopant.[9]

It was recently demonstrated using first principles calculations that substitutional transition metal (TM) atoms can induce a magnetic moment in free-standing graphene.[10,11] For example, substitutional Mo introduces a magnetic moment of 2 μ_B in monolayer graphene.[12] Experimentally, ion irradiation has been shown to produce single C vacancies in graphene, which can be used to trap Fe atoms.[13] The adsorption sites, electronic and magnetic properties of single Fe, Co, and Ni adatoms on monolayer epitaxial graphene (MLEG) on SiC(0001) have been studied by means of STM and X-ray magnetic circular dichroism.[14,15] To obtain well-isolated monomers, the deposition was performed at very low deposition rate and very low substrate temperatures (T = 10 K). However, its two-dimensional nature limits the use of conventional silicon industry substitutional doping methods on graphene. Thus, tuning the electronic properties of graphene, in particular introducing a magnetic moment by individual TM atoms, is still a challenge.

In this article, we demonstrate a simple method to incorporate isolated Mo atoms into BLEG on SiC(0001) and investigate the Mo incorporating sites and corresponding electronic properties of Mo-doped BLEG by means of LT-STM (T = 77 K) and first principles calculations. LT-STM and first principles calculations reveal that isolated substitutional Mo atoms prefer the α-sites of the upper graphene layer and to be embedded between the graphene bilayers. The Mo atoms are stable to ~1100 K because of covalent bonding with neighboring carbon atoms. The first principles calculations show that the Mo atom embedded between graphene bilayers is energetically more stable than that located above the graphene surface. Furthermore, each substitutional Mo atom introduces a magnetic moment of 1.81 μ_B into bilayer graphene.

RESULTS AND DISCUSSION

The ball-and-stick models in Figure 1 (top and side views) show the two inequivalent carbon atoms at α (directly on top of a carbon atom of the layer below) and β (above the center of a carbon hexagon of the layer below) sites. The α and β sites exist in bilayer graphene unit cells due to AB Bernal stacking, which breaks the hexagonal symmetry, as in bulk graphite. The green diamond highlights a unit cell of bilayer graphene with a lattice constant of 2.44 Å. The interlayer distance is 3.34 Å. As the carbon atoms at β sites have a higher local density of states (LDOS) at E_F, three β carbon atoms in each hexagon are observed as protrusions in constant-current STM images,[16] distinct from the 6-fold symmetry of monolayer graphene.[17]

Figure 2 presents large scale representative STM images of EG as-prepared (Figure 2a) and with incorporated Mo atoms (Figure 2b,c) (also refer to Figure S1, Supporting Information). The presence of Mo on the surface is confirmed by *ex situ* photoemission experiments. The two Mo 3*d* related peaks shift from 232.1 and 235.2 eV to 228.6 and 231.7 eV after annealing, suggesting the reduction of Mo^{6+} to Mo (Figure S2, Supporting Information). Unlike on pristine EG where a smooth surface is imaged in STM (with some protrusion-like defects),[17−19] many depressions are observed (at −4 V tip bias) after Mo incorporation. The atomically resolved STM image of such a protrusion-like defect is shown in the inset of Figure S1 (Supporting Information), which is defined as a (carbon) tube-like defect[19] and independent of Mo incorporation. The point defects on BLEG (depressions at −4 V) are imaged as isolated protrusions at 1 V tip bias, as highlighted by red circles in the zoomed-in STM in Figure 2d. Unexpectedly, it is difficult to find similar point defects in MLEG regions (Figure 2d and

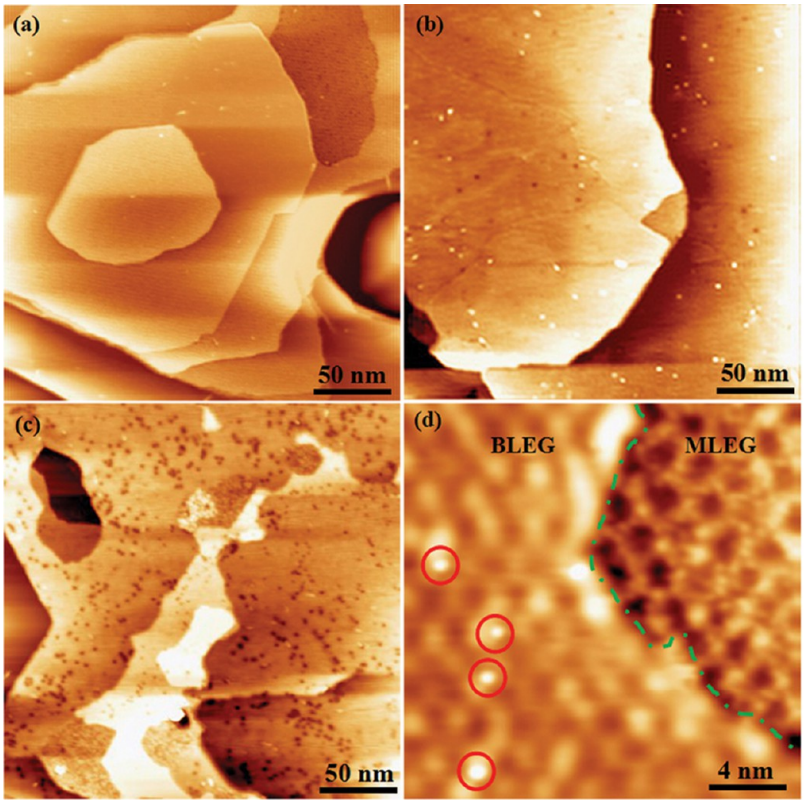

Figure 2. Graphene with randomly dispersed Mo dopants: (a−c) Typical large scale STM image (250 nm × 250 nm) of EG as-prepared (a: V_T = 2 V), with low Mo coverage (b: V_T = −4 V) and higher Mo coverage (c: V_T = −4 V). Depressions randomly distributed over the surface are attributed to incorporated Mo species, while the irregularly shaped bright features are common defects on EG that are independent of Mo incorporation. (d) Zoomed-in STM image (20 nm × 20 nm, V_T = 1 V) indicates isolated Mo dopants (protrusions) highlighted by red circles in BLEG only (please refer to Figure S1, Supporting Information). The dash-dotted curve highlights the boundary between monolayer EG and bilayer EG.

Figure S1b, Supporting Information). For an annealed MoO_3/EG sample (∼1100 K), there are three kinds of defects expected: carbon vacancy, oxygen, and Mo. Carbon vacancies in EG can be ruled out because no obvious 3-fold ($\sqrt{3} \times \sqrt{3}$) pattern is observed around each atomic defect.[16] Chemisorbed oxygen can be removed either by annealing the oxide sample at ∼530 K or by energetic electrons from the STM tip (V_S = 4 V, I_T = 1 nA).[20] For our sample, although it was annealed at ∼1100 K or scanned many times with tip conditions of V_T = −4 V (= $-V_S$), the protrusions are always stable on the surface, excluding the possibility of chemisorbed oxygen. Thus, we propose that these defects are related to isolated Mo dopants in BLEG, as discussed next.

Figure 3a and 3b show high resolution STM images from the same area but at opposite tip bias polarities ((a) V_T = −4 V, (b) V_T = 2 V), highlighting the different appearance of isolated Mo dopants in BLEG. The short rod-like features in both images are related to the tube-like defects in BLEG as above-mentioned.[19] The depressions (Figure 3a) or protrusions (Figure 3b) with radial symmetry are attributed to isolated Mo dopants. While the depressions have maximum lateral dimensions (fwhm: full width at half-maximum) of 22.5 ± 0.5 Å and an apparent maximum height of ∼ −1.8 Å with respect to the BLEG surface, the protrusions possess maximum lateral dimensions of 8.5 ± 0.5 Å and an apparent maximum height of ∼3.0 Å, as shown in the corresponding line profiles in Figure 3c and 3d. The apparent height difference (either in Figure 3c or in Figure 3d) can be attributed to the different Mo adsorption sites in BLEG relative to the underlying reconstructed SiC surface. For chemisorbed atomic oxygen on EG, the lateral diameter of the oxygen features observed in the STM images is ∼12 Å, which is attributed to oxygen chemisorption-induced topographic distortion of EG in the region surrounding the oxygen bonding site.[20] The larger protrusions corresponding to Mo may arise for a similar reason: Mo incorporation induces topographic distortion of EG in the region surrounding the Mo bonding site. The depressions in the empty state STM images cannot be attributed to the electronic interaction of Mo atom with neighboring C atoms but to a local change of tip-induced-band-bending (TIBB) arising from the presence of the Mo atom. For *n*-type BLEG[21,22] at negative tip bias, a tip-induced band bending enables electron tunneling from the tip to the substrate. However, electron tunneling may be inhibited if the band

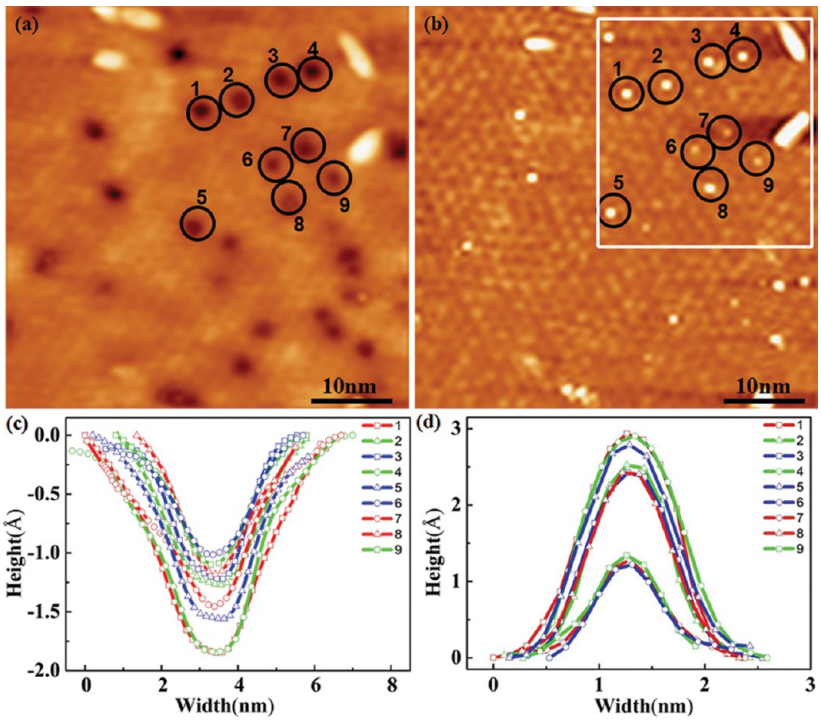

Figure 3. Zoomed-in STM images from the same area (50 nm × 50 nm) but at opposite tip bias polarities ((a) $V_T = -4$ V, (b) $V_T = 2$ V) showing the different appearance of Mo dopants in BLEG. Panels (c) and (d) show the line profiles across nine circled and numbered dopants in (a) and (b), respectively.

bending is locally reduced due to electrostatic effects of the Mo atom. The tip must therefore move closer to the surface to compensate. Thus, the Mo atom appears as a depression. The magnitude of local change in TIBB depends on the lateral distance between the tip and the position of the Mo atom. With increasing distance, the influence of electrostatic effects of Mo atom on TIBB decreases. Therefore, a circular depression occurs around the position of Mo atom in the STM image.[23,24] A similar impurity-induced electronic effect on electron tunneling has been reported for STM images of Fe dopants in the subsurface region of H−Si(111)[23] and Ga adatom on GaAs.[25]

To determine the geometrical structure of Mo incorporated BLEG, atomically resolved STM is helpful. Figure 4a shows an atomically resolved STM image taken from the white square labeled in Figure 3b showing both the isolated Mo dopants and the tube-like defects on BLEG. The atomic feature of Mo dopants is different from that of Co or Ni adatoms on MLEG on SiC(0001), where ~3-Å-high protrusions extending over several honeycombs on graphene are observed for single Co or Ni adatoms at the tip bias in the range of −0.5 to 0.5 V.[14] This suggests that Mo atom is not adsorbed on top of but incorporated into BLEG. Theoretical calculations using the climbing-image nudged elastic band method predict that the energy barrier for a Pd atom going through a single atomic defect in a Ru(0001) supported graphene is only 0.49 eV.[26] It is reasonable that the reduced Mo atoms can overcome a comparative energy barrier at ~1100 K and go through the top graphene layer at the atomic defect site, which is created during the reduction of MoO_3 on EG surface. The covalent bond between Mo atom and nearest three C atoms makes them indistinguishable in the close-up STM image in Figure 4b, where a characteristic triangular structure occurs at the doping site and the triangular lattice of BLEG remains intact. The length of this triangle is equal to the graphene lattice constant (~2.5 Å); *i.e.*, there is almost no distortion. According to the triangular lattice of BLEG, it is obvious that each apex of such triangle is located at a C atom of the same sublattice. The line profile taken along the dash-dotted line through the dopant (Figure 4b) yields a maximum apparent out-of-plane height of 0.5 ± 0.1 Å. This is similar to the case of individual nitrogen dopants in CVD grown graphene,[8] indicating that the Mo atom is actually incorporated into BLEG. As above-mentioned, only carbon atoms at β sites can be visualized in constant current STM images due to their higher LDOS at E_F. Since all the local density of states (LDOSs) of β atoms and a small percentage of those of α atoms can be detected,[27] α and β atoms can be identified in the line profile superimposed in Figure 4b by cyan and yellow arrows, respectively, indicating that the center of the triangle is located at α sites. Figure 4c is a corresponding model where a graphene layer is superimposed on the same STM image as in Figure 4b accordingly, confirming that Mo atom substitutes one carbon atom at α sites. Since the covalent radii

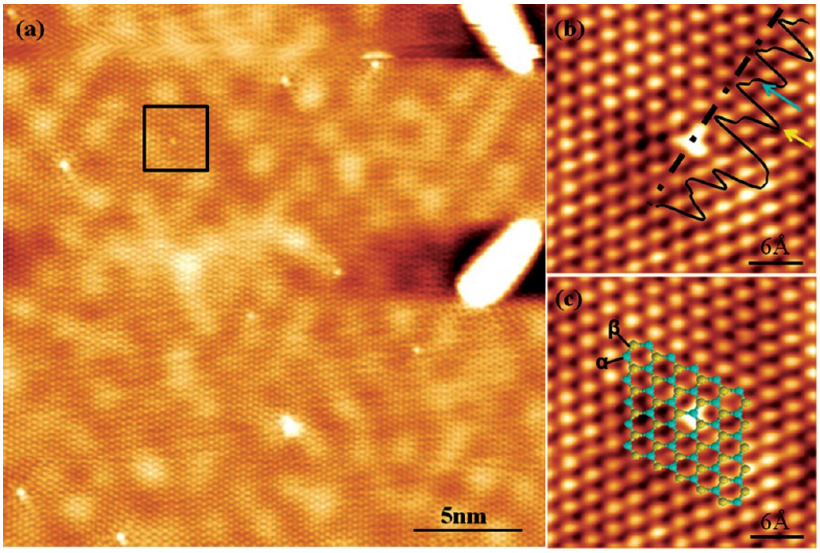

Figure 4. (a) Atomically resolved STM image (25 nm × 25 nm, V_T = 0.5 V) taken from the white square region in Figure 3b. No apparent scattering is observed around the isolated Mo dopants. (b) A representative zoomed-in STM image (3 nm × 3 nm, V_T = −0.3 V) of a Mo dopant in the BLEG. The line-profile taken along the dash-dotted line through the dopant indicates α-site adsorption of Mo: yellow arrow for β site and cyan arrow for α site. (c) Same as (b): superimposed with schematic top view on the atomic structure of graphene.

of TM atoms are larger than those of C atoms, the substitutional TM atoms are displaced from the graphene plane, inducing a local curvature of graphene. Taking no Mo dopants in MLEG region and the small apparent height of ~0.5 Å into account, we postulate that the α-site substitutional Mo atom is located between the two graphene layers in BLEG.

To further confirm the proposed configuration of a Mo atom at the substitutional α site and embedded between BLEG, as well as to predict the corresponding electronic properties, first-principles calculations within the framework of density functional theory (DFT) are carried out. Four substitutions with higher symmetry (possibilities) as shown in Figure S3 (Supporting Information) are studied, which are defined as configurations a−d, respectively. Note that this BLG model neglects the substrate effect of BLEG. According to the calculated binding energies, it is found that configurations b and d (where Mo atoms substitute carbon atoms at α and β site, respectively, and located out of bilayer graphene) are energetically less favorable than configurations a and c (where Mo atoms substitute carbon atoms at α and β site, respectively, and located in between bilayer graphene), in good agreement with STM observations. However, in contrast to the experimental result, the binding energy of configuration c is 0.31 eV lower than that of configuration a, indicating Mo is more stable at the β site between freestanding bilayer graphene. The Mo atom in configuration c is directly above the hollow site of lower graphene layer, leading to a much smaller interlayer distance and deformation. This is why configuration a is less favorable than configuration c in the calculation. In addition to the inadequate description of intermolecular weak interaction energy by the DFT method and the limited size of the calculation model, two other important factors may contribute to this contradiction. One is that the underlying SiC substrate can induce n-doping and corrugation of BLEG, which may significantly affect EG properties.[28] For example, recent LT-STM investigations reveal that Ni and Co adatoms were adsorbed at different sites on pristine and quasi-free-standing MLEG, indicating that the underlying substrate plays a crucial role in determining the adsorption site as well as the electronic properties of TM adatoms on graphene.[14,15] Another possible explanation is that the Mo substitution reaction at the α site may undergo a lower energy barrier than at the β site, even though its product is thermodynamically unfavorable. Further experimental and theoretical studies are needed to better understand this issue.

Figure 5 summarizes the calculated atomic and electronic structures of Mo-doped free-standing bilayer graphene (BLG) in configuration a. Since the Mo atom has a much larger van der Waals radius than the carbon atom, the interlayer distance of BLG is increased from 3.3 to 3.6 Å (Figure S3, Supporting Information). Obvious deformation of the lower graphene layer is observed, as shown in Figure 5a. A net magnetic moment of 1.81 μ_B is obtained, and the density of net spin as shown in Figure 5c demonstrates that the magnetic moment is completely localized at the Mo atom. The DOSs (Figure 5d) show that the Mo dopant causes bilayer graphene to undergo a semimetal to metal transition due to the Mo shallow *d* bands near E_F. The net magnetic moment is mainly contributed by the sharp peak slightly below E_F

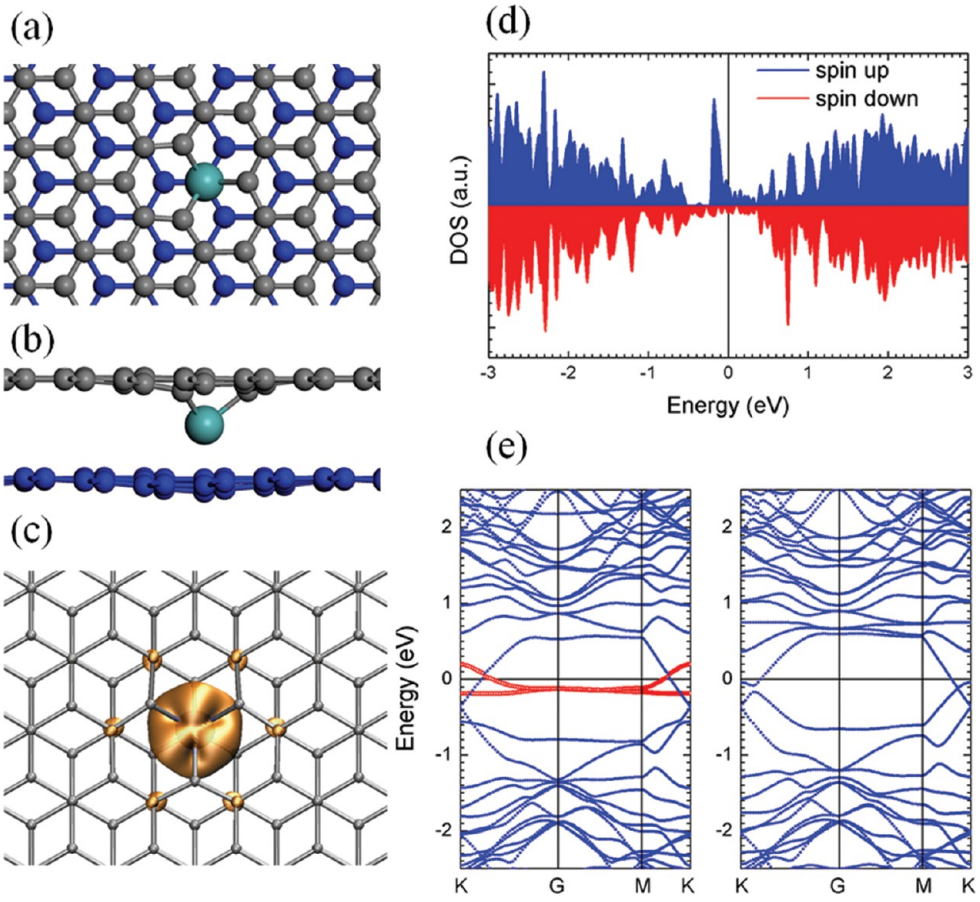

Figure 5. (a) Top and (b) side views of optimized structure of BLG with Mo-substituted at α site and between the two free-standing BLG layers. (c) Spatial distribution of spin-polarized charge density (spin up minus spin down). (d) Density of states. (e) Band structures (left, spin up; right, spin down). Red lines highlight the localized spin state of the two flat bands around E_F.

corresponding to the 4*d* bands of Mo. This localized spin state is also reflected by two flat bands around E_F in the band structure (red lines in Figure 5e). It is also clear that these two *d* bands of Mo atom, as well as E_F, are 0.3 eV above the Dirac point of graphene, indicating the BLG is n-doped.

CONCLUSION

In conclusion, we have demonstrated the possibility of incorporating single transition metal (Mo) dopants into bilayer graphene in a stable configuration. Scanning tunneling microscopy results show that the substitutional Mo dopants prefer to embed inside bilayer graphene and the electronic structure of graphene is strongly modified only within a few lattice spacings of the Mo dopant site. DFT calculations show that each Mo atom introduces a local magnetic moment of 1.81 μ_B into BLEG. This single Mo-doped bilayer graphene structure may be incorporated into the design of novel graphene spintronics devices.

METHODS

All the experiments were carried out in a custom-built multichamber ultrahigh vacuum (UHV) system housing an Omicron low-temperature scanning tunneling microscope (LT-STM) with base pressure better than 6.0×10^{-11} mbar.[17] The EG samples (MLEG and BLEG coexist) were prepared by thermal decomposition of a chemically etched n-type Si-terminated 4H-SiC-(0001) sample (CREE Research Inc.) at 1500 K in UHV.[17,18] The quality of EG was confirmed by *in situ* LT-STM. MoO_3 was evaporated *in situ* from a Knudsen cell onto EG at room temperature in the growth chamber. The nominal deposition rate of MoO_3 (0.2 nm/min) was precalibrated by a quartz crystal microbalance.[29] By annealing the sample gradually up to about 1100 K and maintaining the temperature for 10 min, some Mo atoms decomposed from MoO_3 and incorporated into BLEG. The sample temperatures were measured by an optical pyrometer. All STM images were recorded in constant current mode using chemically etched tungsten (W) tips at 77 K. The low temperature used minimized thermal noise to give atomically resolved STM images, which were analyzed using WSxM software.[30]

For the first principles calculation, a 5×5 supercell of BLG is used with the vacuum space of 20 Å. van der Waals corrected Becke88 functional (optB88-vdW)[31] is employed to better describe the weak interlayer interaction of BLG. The project argument wave function (PAW) pseudopotential is used with energy cutoff for plane wave basis setting as 400 eV. The first Brillouin zone is sampled by $5 \times 5 \times 1$ k-points using the Monkhorst-Pack scheme in geometry optimization, and $15 \times 15 \times 1$ k-points in DOS and bandstructure calculation.

All the calculations are performed by Vienna *Ab Initio* Simulation Package (VASP).[32−35]

Conflict of Interest: The authors declare no competing financial interest.

Supporting Information Available: STM image of Mo incorporated sample with the coexistence of MLEG and BLEG. Synchrotron-based high-resolution *ex situ* Mo 3*d* spectra as a function of annealing temperature. Calculated configurations of Mo incorporated BLG. This material is available free of charge *via* the Internet at http://pubs.acs.org.

Acknowledgment. We are grateful to Prof. C. I. Pakes, Department of Physics, La Trobe University, and A. Tadich, at the Australian Synchrotron, for their assistance on the *ex situ* PES experiments. We acknowledge the financial support from NRF-CRP Grants R-143-000-360-281: "Graphene and Related Materials and Devices" and R-144-000-295-281: "Novel 2D materials with tailored properties—beyond graphene". Dr. Han Huang acknowledges the "Shenghua Professorship" startup funding from Central South University and the support from the NSF of China (Grant No.11304398).

REFERENCES AND NOTES

1. Geim, A. K.; Novoselov, K. S. The Rise of Graphene. *Nat. Mater.* **2007**, *6*, 183–191.
2. Geim, A. K. Graphene: Status and Prospects. *Science* **2009**, *324*, 1530–1534.
3. Banhart, F.; Kotakoski, J.; Krasheninnikov, A. V. Structural Defects in Graphene. *ACS Nano* **2011**, *5*, 26–41.
4. Rutter, G. M.; Crain, J. N.; Guisinger, N. P.; Li, T.; First, P. N.; Stroscio, J. A. Scattering and Interference in Epitaxial Graphene. *Science* **2007**, *317*, 219–222.
5. Lahiri, J.; You, L.; Bozkurt, P.; Oleynik, I. I.; Batzill, M. An Extended Defect in Graphene as a Metallic Wire. *Nat. Nanotechnol.* **2010**, *5*, 326–329.
6. Ugeda, M. M.; Brihuega, I.; Guinea, F.; Gomez-Rodriguez, J. M. Missing Atom as a Source of Carbon Magnetism. *Phys. Rev. Lett.* **2010**, *104*, 096804.
7. Ugeda, M. M.; Fernandez-Torre, D.; Brihuega, I.; Pou, P.; Martinez-Galera, A. J.; Perez, R.; Gomez-Rodrguez, J. M. Point Defects on Graphene on Metals. *Phys. Rev. Lett.* **2011**, *107*, 116803.
8. Zhao, L. Y.; He, R.; Rim, K. T.; Schiros, T.; Kim, K. S.; Zhou, H.; Gutierrez, C.; Chockalingam, S. P.; Arguello, C. J.; Palova, L.; *et al.* Visualizing Individual Nitrogen Dopants in Monolayer Graphene. *Science* **2011**, *333*, 999–1003.
9. Zhao, L. Y.; Levendorf, M.; Goncher, S.; Schiros, T.; Palova, L.; Zabet-Khosousi, A.; Rim, K. T.; Gutierrez, C.; Nordlund, D.; Jaye, C.; *et al.* Local Atomic and Electronic Structure of Boron Chemical Doping in Monolayer Graphene. *Nano Lett.* **2013**, *13*, 4659–4665.
10. Mao, Y. L.; Yuan, J. M.; Zhong, J. X. Density Functional Calculation of Transition Metal Adatom Adsorption on Graphene. *J. Phys.: Condens. Matter* **2008**, *20*, 115209.
11. Mao, Y. L.; Zhong, J. X. Structural, Electronic and Magnetic Properties of Manganese Doping in the Upper Layer of Bilayer Graphene. *Nanotechnology* **2008**, *19*, 205708.
12. Kang, J.; Deng, H. X.; Li, S. S.; Li, J. B. First-Principles Study of Magnetic Properties in Mo-Doped Graphene. *J. Phys.: Condens. Matter* **2011**, *23*, 346001.
13. Robertson, A. W.; Montanari, B.; He, K.; Kim, J.; Allen, C. S.; Wu, Y. A.; Olivier, J.; Neethling, J.; Harrison, N.; Kirkland, A. I.; *et al.* Dynamics of Single Fe Atoms in Graphene Vacancies. *Nano Lett.* **2013**, *13*, 1468–1475.
14. Eelbo, T.; Wasniowska, M.; Gyamfi, M.; Forti, S.; Starke, U.; Wiesendanger, R. Influence of the Degree of Decoupling of Graphene on the Properties of Transition Metal Adatoms. *Phys. Rev. B* **2013**, *87*, 205443.
15. Eelbo, T.; Wasniowska, M.; Thakur, P.; Gyamfi, M.; Sachs, B.; Wehling, T. O.; Forti, S.; Starke, U.; Tieg, C.; Lichtenstein, A. I.; *et al.* Adatoms and Clusters of 3*d* Transition Metals on Graphene: Electronic and Magnetic Configurations. *Phys. Rev. Lett.* **2013**, *110*, 136804.
16. Kibsgaard, J.; Lauritsen, J. V.; Laegsgaard, E.; Clausen, B. S.; Topsoe, H.; Besenbacher, F. Cluster-Support Interactions and Morphology of MoS_2 Nanoclusters in a Graphite-Supported Hydrotreating Model Catalyst. *J. Am. Chem. Soc.* **2006**, *128*, 13950–13958.
17. Huang, H.; Chen, W.; Chen, S.; Wee, A. T. S. Bottom-up Growth of Epitaxial Graphene on 6H-SiC(0001). *ACS Nano* **2008**, *2*, 2513–2518.
18. Huang, H.; Chen, S.; Gao, X. Y.; Chen, W.; Wee, A. T. S. Structural and Electronic Properties of PTCDA Thin Films on Epitaxial Graphene. *ACS Nano* **2009**, *3*, 3431–3436.
19. Wang, Q. H.; Hersam, M. C. Room-Temperature Molecular-Resolution Characterization of Self-Assembled Organic Monolayers on Epitaxial Graphene. *Nat. Chem.* **2009**, *1*, 206–211.
20. Zakir Hossain, M.; Johns, J. E.; Bevan, K. H.; Karmel, H. J.; Liang, Y. T.; Yoshimoto, S.; Mukai, K.; Koitaya, T.; Yoshinobu, J.; Kawai, M.; *et al.* Chemically Homogeneous and Thermally Reversible Oxidation of Epitaxial Graphene. *Nat. Chem.* **2012**, *4*, 305–309.
21. Ohta, T.; Bostwick, A.; McChesney, J. L.; Seyller, T.; Horn, K.; Rotenberg, E. Interlayer Interaction and Electronic Screening in Multilayer Graphene Investigated with Angle-Resolved Photoemission Spectroscopy. *Phys. Rev. Lett.* **2007**, *98*, 206802.
22. Lauffer, P.; Emtsev, K. V.; Graupner, R.; Seyller, T.; Ley, L. Atomic and Electronic Structure of Few-Layer Graphene on SiC(0001) Studied with Scanning Tunneling Microscopy and Spectroscopy. *Phys. Rev. B* **2008**, *77*, 155426.
23. Gruyters, M.; Pingel, T.; Berndt, R. Subsurface Sites of Fe in H/Si(111) Studied by Scanning Tunneling Microscopy. *Phys. Rev. B* **2013**, *87*, 165405.
24. Brar, V. W.; Brar, V. W.; Decker, R.; Solowan, H. M.; Wang, Y.; Maserati, L.; Chan, K. T.; *et al.* Gate-Controlled Ionization and Screening of Cobalt Adatoms on a Graphene surface. *Nat. Phys.* **2011**, *7*, 43–47.
25. Gohlke, D.; Mishra, R.; Restrepo, O. D.; Lee, D.; Windl, W.; Gupta, J. Atomic-Scale Engineering of the Electrostatic Landscape of Semiconductor Surfaces. *Nano Lett.* **2013**, *13*, 2418–2422.
26. Huang, L.; Pan, Y.; Pan, L.; Gao, M.; Xu, W. Y.; Que, Y.; Zhou, H. T.; Wang, Y. L.; Du, S. X.; Gao, H. J. Intercalation of Metal Islands and Films at the Interface of Epitaxially Grown Graphene and Ru(0001) Surfaces. *Appl. Phys. Lett.* **2011**, *99*, 163107.
27. Tomanek, D.; Louie, S. G.; Mamin, H. J.; Abraham, D. W.; Thomson, R. E.; Ganz, E.; Clarke, J. Theory and Observation of Highly Asymmetric Atomic Structure in Scanning-Tunneling-Microscopy Images of Graphite. *Phys. Rev. B* **1987**, *35*, 7790–7793.
28. Huang, H.; Wong, S. L.; Sun, J.; Chen, W.; Wee, A. T. S. Trapping Single Polar Molecules in SiC Nanomesh *via* Out-of-Plane Dipoles. *ACS Nano* **2012**, *6*, 2774–2778.
29. Chen, Z. Y.; Santoso, I.; Wang, R.; Xie, L. F.; Mao, H. Y.; Huang, H.; Wang, Y. Z.; Gao, X. Y.; Chen, Z. K.; Ma, D. G.; *et al.* Surface Transfer Hole Doping of Epitaxial Graphene Using MoO_3 Thin Film. *Appl. Phys. Lett.* **2010**, *96*, 213104.
30. Horcas, I.; Fernandez, R.; Gomez-Rodriguez, J. M.; Colchero, J.; Gomez-Herrero, J.; Baro, A. M. WSXM: A Software for Scanning Probe Microscopy and a Tool for Nanotechnology. *Rev. Sci. Instrum.* **2007**, *78*, 013705.
31. Klimes, J.; Bowler, D. R.; Michaelides, A. Chemical Accuracy for the Van Der Waals Density Functional. *J. Phys.: Condens. Matter* **2010**, *22*, 022201.
32. Kresse, G.; Furthmüller, J. Efficiency of *Ab-Initio* Total Energy Calculations for Metals and Semiconductors Using a Plane-Wave Basis Set. *Comput. Mater. Sci.* **1996**, *6*, 15–50.
33. Kresse, G.; Hafner, J. *Ab Initio* Molecular Dynamics for Liquid Metals. *Phys. Rev. B* **1993**, *47*, 558–561.
34. Kresse, G.; Furthmüller, J. Efficient Iterative Schemes for *Ab Initio* Total-Energy Calculations Using a Plane-Wave Basis Set. *Phys. Rev. B* **1996**, *54*, 11169–11186.
35. Kresse, G.; Joubert, D. From Ultrasoft Pseudopotentials to the Projector Augmented-Wave Method. *Phys. Rev. B* **1999**, *59*, 1758–1775.